Conference paper

Concentrating Solar Thermal Process Heat for Manganese Ferroalloy Production: Plant Modelling and Thermal Energy Storage Dispatch Optimization

This paper presents a modelling tool to help with the design of CSP power towers. The tool assumes the heat will be used to preheat manganese ferroalloy.

Responsible partner: SUN

This project has received funding form the European Union's Horizon 2020 research and innovation programme under grant agreement No 820561

PREMA PROJECT OVERVIEW

The PREMA project has received funding from the European Union's Horizon 2020 Research and Innovation Programme under Grant Agreement No 820561. PREMA is an H2020 project that aims to reduce the energy consumption and CO2 emissions from manganese production. The plan is to preheat manganese ore with industrial off-gases and solar thermal energy, which will reduce the amount of electricity and coal required to smelt the ore.

The work presented here has been funded by the PreMa project.

Proceedings of the ASME 2020
14th International Conference on Energy Sustainability
ES2020
June 8-10, 2020, Denver, CO, USA

ES2020-6654

CONCENTRATING SOLAR THERMAL PROCESS HEAT FOR MANGANESE FERROALLOY PRODUCTION: PLANT MODELLING AND THERMAL ENERGY STORAGE DISPATCH OPTIMIZATION

Tristan Mckechnie[1], Craig McGregor, Gerhard Venter
Department of Mechanical and Mechatronic Engineering, Stellenbosch University
Stellenbosch, Western Cape, South Africa

ABSTRACT

This paper investigates the economic benefit of incorporating solar-based preheating of Manganese ore before smelting in electric submerged arc furnaces. Manganese ore is smelted to produce Manganese ferroalloy, a key component in steel production. The smelting process is highly energy intensive, with temperatures up to 1600 ℃*. The paper discusses the developed methodology for determining the configuration of a concentrating solar thermal (CST) plant to produce high temperature process heat. The CST plant is sized to preheat the ore to* 600 ℃ *before it enters the smelter – currently ore enters at ambient temperature. The preheating leads to economic and environmental benefits by offering lower cost heat and reducing carbon emissions for the process.*

Keywords: Concentrating solar thermal, industrial process heat, dispatch optimization.

NOMENCLATURE

SM	Solar multiple
$\dot{Q}$	Thermal power [W]
Q	Thermal energy [Wh]
$\dot{x}$	Thermal energy storage dispatch [W]
C	Electrical tariff [$/kWh]
CST	Concentrating solar thermal
TES	Thermal energy storage
LCOH	Levelized cost of heat
η	Efficiency
DLR	German Aerospace Center's Institute for Solar Research
STERG	Solar Thermal Energy Research Group from Stellenbosch University
DNI	Direct Normal Irradiance

1. INTRODUCTION

Renewable energy sources are achieving increasing levels of market penetration in the global electricity sector. REN21's 2019 global status report states that by the end of 2016 26 % of the global electricity was supplied by renewable energy, and for the years 2014 – 2018 more than 50 % of the annual additional electrical generating capacity was from renewable energy sources [1]. However, the same report states that renewable energy represents only 9.8 % and 3.3 % of the total heating and cooling, and transport, energy use respectively. If the world is to meet the climate goals of the Paris Accord renewable energy technologies must achieve greater market penetration in these sectors.

Industrial process heat represents a large portion of world energy use and is a sector that could see greater integration of renewable technologies. Concentrating solar technologies are a well-established technology, suited to meeting the need for high temperature industrial process heat as it is capable of generating heat in excess of 1000 °C [2].

This paper investigates the use of CST energy from an embedded generation plant to preheat manganese ore prior to smelting operations. This leads to energy savings in the furnace and carbon emission reductions. Manganese smelting occurs at temperatures up to 1600 °C [3]. For this reason CST technologies are well suited to the problem due its capabilities of generating high temperature heat. A hybrid CST-electric plant concept, capable of delivering heat for preheating ore with a 100 % capacity factor, ensuring steady furnace operating conditions, is introduced. Additionally, the TES dispatch profile is determined to minimize the cost of electrical heat, ensuring a minimal combined levelized cost of solar-electric heat.

The paper describes the model and methodologies developed to simulate plant performance and determine plant

[1] Contact author: 18976697@sun.ac.za

configuration. After which a case study for such a plant is developed to investigate the benefit that can achieved.

2. BACKGROUND

The research presented in this paper is funded by the PREMA project, an EU Horizon 2020 project focused on improving the energy efficiency of Manganese smelting processes by preheating ore before its enters the furnace [4]. Due to the high temperatures involved in the smelting processes, CST technologies have been identified as a suitable solution to deliver the high temperature process heat necessary to preheat ore before smelting. This paper investigate the application of the PREMA project's partner's selected technologies, namely the CentRec® particle receiver and HelioPod™ heliostat, to the concept of a CST plant delivering process heat to a Manganese smelter.

2.1 High temperature solar derived process heat

Central receiver technologies making use of solid particles as the heat transfer medium are capable of achieving temperatures above 1000 °C, higher than current molten salt technologies [5]. Several papers have been published regarding the use of particle receivers to generate high temperature process heat for industrial processes.

Researchers from the DLR have published several papers investigating solar derived process heat for use in various industrial applications and replacing various heat sources. The work is centered on the CentRec® particle receiver, which is capable of heating particles to 900 °C and providing process heat at 750 °C. Amsbeck et al [6] investigated the use of a CST plant to deliver heat to a plasterboard manufacturer for the drying of plasterboard. The solar derived heat proved to be cost competitive against liquid fuels for a plant modelled in Australia. Amsbeck et al [7] investigated solar pre-heating of minerals prior to smelting operations in induction furnaces. A case study for a 12 MW_e induction furnace located in Brazil determined that delivering hot air to preheat the minerals prior to smelting saves up to one-third of the furnace's electrical load. The CST plant achieved payback in just over four years. Lubkoll et al [8] investigated the incorporation of solar derived preheating of Manganese ore prior to sintering operations. The ore is sintered to increase the Manganese content of the product. The solar heat replaced heat supplied by a combination of diesel and coke combustion. The CST plant was capable of delivering the required heat for significantly lower cost than burning diesel.

Compared to the previous discussed papers, a major difference in this paper is that that Manganese preheating requires constant heat availability. This leads to a requirement for backup electric heaters, which gives rise to an optimization problem tied to the optimal timing for dispatch of thermal energy.

2.2 Manganese smelting

Manganese ore is smelted to produce Manganese ferroalloys, which is predominantly used as a component in steelmaking[9]. The ore is commonly smelted in Submerged Arc Furnaces, where electricity provides the energy to reach the high smelting temperatures of up to 1600 °C [9]. In South Africa furnaces range between 15-45 MW_e each and operate near continuously year round, making for an extremely energy intensive industry.

The goal of the PREMA project is to preheat Manganese ore to 600 °C. Tangstad et al [3] determined this can reduce the energy consumption of the furnace by more than 20 %. Additionally, if electricity is sourced from non-renewable sources there is potential for a significant decrease in carbon emissions by reducing the furnace energy consumption, if the preheating energy is delivered by a renewable source.

3. SYSTEM COMPONENTS

This section discusses the solar technologies of the PREMA project's partner organizations and the parameters required for modelling these technologies. STERG's heliostat technology and the DLR's particle receiver, thermal storage and particle-to-air heat exchanger are to be investigated for achieving solar thermal preheating of the ore.

3.1 HelioPod™

STERG has developed the HelioPod™ heliostat technology [10]. Figure 1 shows the HelioPod™. There are six individual, single panel facets on a shared base structure. The structure requires no foundations and has autonomous calibration capabilities to correct for any positional changes with time. The heliostat tracking is powered from small onboard PV panels and therefore no trenching for cabling is required. These characteristics make the HelioPod™ a mobile and fast solution to implement. Table 1 provides the optical properties of the HelioPod™ technology required for modelling, as given by Lubkoll et al [8].

Figure 1: HelioPod™ technology.

Table 1: Optical parameters used to model solar field.

Parameter	Value
# Heliostats per pod	6
Facet aperture dimensions	1.83 m × 1.22 m
Facet focal length	Variable
Surface slope and tracking error	≤ 1.5 mrad
Reflectivity	95 %

3.2 Particle receiver

The DLR has developed the CentRec® particle receiver capable of reaching temperatures of 1000 °C [11]. The operating principles of the receiver is explained by Wu et al[12]. The receiver is tilted downward from the horizontal, and rotates while particles are fed from above. The particles move uniformly downward on the cavity wall due to the combination of gravitational and centrifugal forces. Reflected irradiation enters through an aperture to heat the particles. The rate of rotation is varied to control the exposure time of the particles to the incoming irradiation, thereby ensuring the particles reach the desired temperature under different load conditions.

Lab scale proof of concept tests conducted by Wu et al [13] have confirmed that particle outlet temperatures of 900 °C can be achieved under a variety of incoming solar fluxes by controlling the particle mass flow rate. Ebert et al [14] discuss the experience gained from full scale testing of a 2.5 MW_{th} prototype. The prototype completed over 70 hours of on-sun testing, confirming the ability to heat ceramic particle to an average outlet temperature of 900 °C for a sustained periods.

Figure 2 depicts the operating principle and the thermal efficiency of the CentRec® receiver. Wu et al [12] developed a numerical model of a 1 MW/m^2 receiver to determine the thermal efficiency as a function of incident flux. The model was validated against lab scale prototype tests. The same data is not available for the 2.5 MW/m^2 receiver used in this paper. To account for thermal losses under varying conditions, the same data as in Figure 2 will be used to model the receiver, with the assumption that at flux exceeding 1 MW/m^2 the efficiency remains constant. This represents a conservative approach as reported full load efficiency of the commercially sized receiver is in excess of 90 % [7]. Furthermore for the relatively small field modelled, the receiver is predominantly operated under full load conditions.

A discussion of different particle receiver technologies is provided by Ho[5]. Modelling results for a falling particle receiver from Ho et al [15] report similarly high thermal efficiency, ~ 90 % for high input flux conditions.

The parameters used for modelling the receiver are presented in Table 2.

Table 2: Parameters required for modelling the thermal performance of the CentRec® receiver.

Parameter	Value
Aperture area[1]	1 m^2
Outlet temperature[1]	900 °C
Maximum thermal rating[1]	2.5 MW_{th}
Tower height[2]	40 m
Tilt angle[2]	45°

[1] CentRec® commercial configuration [16], [2] modelled by Lubkoll et al [8]

3.3 Solid particle thermal energy storage

The thermal energy storage (TES) consist of two insulated particle storage bins, a hot and cold bin. Palacios et al [17] reports this storage concept is capable of storage temperatures in excess of 1000 °C whilst using low-cost materials. El-Leathy et al [18] published test findings of a small scale rectangular particle storage bin consisting of insulating firebrick and concrete. The daily heat loss was reported to be 4.4 %. Al-Ansary et al [19] used these results to further develop the concept, introducing a cylindrical bin consisting of a concrete and refractory cement construction. The authors published results of a numerical model for this new design, where the daily heat loss was reported to be 4.3 %. El-Leathy and Al-Ansary both predict the heat loss to reduce to 1 % for a utility-scale TES bin. Therefore the hourly heat loss is modelled as an hourly thermal efficiency, η_{TES} for the TES.

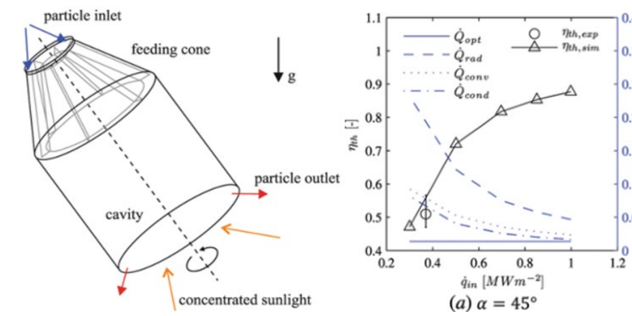

Figure 2: CentRec® particle receiver operating principles[12].

3.4 Particle-to-air heat exchanger

In the paper by Hertel et al [20] the DLR propose a moving bed direct contact particle-to-air heat exchanger. Hot particles from storage are used to heat air, which will then be used to preheat the Manganese ore. The particles enter the heat exchanger from storage at 900 °C and heat the air to 750 °C. The Manganese ore is then expected to be heated to 600 °C prior to preheating. The expectation that this configuration of solar plant is capable of providing the above temperatures is in agreement with the modeling of Amsbeck et al [6], Amsbeck et al [7] and Lubkoll et al[8].

4. MODEL AND METHODOLOGY

This section describes the development of the pseudo steady-state model used to simulate the operation of the CST plant. Figure 3 shows the hybrid CST-electric plant layout. The plant consists of the solar field, receiver, thermal energy storage, back-up electrical heaters and a particle-to-air heat exchanger.

Incorporating preheating into furnace operations requires that ore is always preheated, in order to keep the furnace operating conditions and control steady. Therefore the output from the CST-electric plant must be constant, hence the addition of backup electrical heaters.

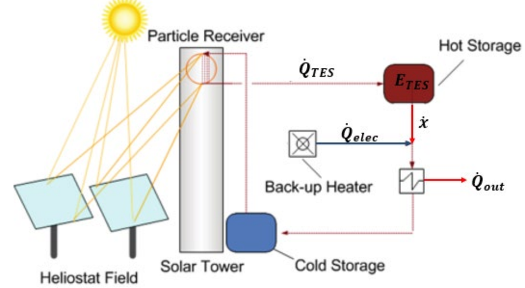

Figure 3: CST plant layout (adapted from [21]).

4.1 Solar field sizing

The number of heliostats required in the solar field is determined with the sun's locations at solar noon at spring/autumn Equinox and a design DNI of $1000\ \mathrm{W \cdot m^{-2}}$, to provide 2.5 $\mathrm{MW_{th}}$ to the receiver. The size of a solar field is typically reported as the solar multiple. Solar multiple is defined by Lovegrove and Stein [2] as:

$$SM = \frac{\dot{Q}_{des,field}}{\dot{Q}_{des,process}}, \quad (1)$$

where $\dot{Q}_{des,field}$ will be 2.5 $\mathrm{MW_{th}}$ as this is the commercial thermal rating of the receiver and the field is sized to deliver this under design conditions. Typically the denominator is the constraint on equation 1 (a thermal requirement for a desired turbine size in a concentrating solar power plant) but due to the selection of the CentRec® receiver and its limitation to the reported commercial size of 2.5 $\mathrm{MW_{th}}$, the numerator is the constraint and so the output to process will be the subject of investigation in later discussion.

4.2 Field layout

The heliostat field is predominantly a polar field (heliostats located only north/south of the receiver), with some located behind the tower. As the receiver is tilted downward, some heliostats behind and to the side of the tower have line of site to the receiver aperture. Placing the tower slightly inside in the field increases the field optical efficiency by minimizing attenuation and spillage loses. The use of the CentRec® receiver limits the field to a predominantly polar layout.

The field layout was developed by Lubkoll et al [8] and can be described as rows of staggered and tessellated HelioPods™ placed within a bounding circle. This field layout is practical to produce with the HelioPod™ technology due to its triangular base structure. Figure 5 shows the field layout. The tower is located at the red dot.

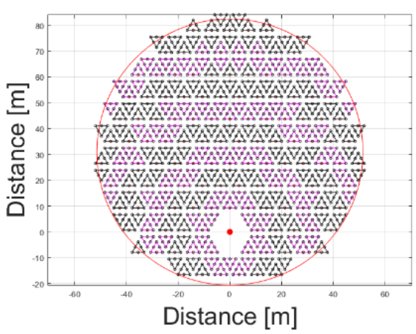

Figure 4: HelioPod™ field layout.

4.3 Optical model

The optical model determines the amount of irradiation that is successfully intercepted by the solar field, and reflected to the receiver. This is simulated using a solar ray-tracing software, which incorporates the geometry and optics of the heliostats, the field layout and the sun's varying position and irradiation. In this paper Tonatiuh©, a validated open source ray-tracing software is used [22].

Simulating the solar field yields the optical efficiency parameter. The optical efficiency is the percentage of solar irradiation intercepted by the heliostats that is successfully reflected onto the receiver. The optical efficiency accounts for blocking, shading, spillage, atmospheric attenuation, cosine and reflectivity losses as explained by Stine and Geyer [23].

CSP plant simulation is typically completed with an hourly resolution for a single year [24]. To decrease computational expense associated with ray-tracing an interpolation method is implemented where only three days are simulated with hourly resolution. From this an interpolation model is created to determine the optical efficiency as a function the sun's location. The optical efficiency at any other moment in time can then be calculated without the expense of running the ray-tracing simulation. This approach is implemented by the solar ray-tracer SolarPilot [24], as well by Lubkoll et al [8].

To generate the interpolation model the summer and winter solstices and autumn/spring equinox are used. These days represents times where the sun is at its extreme location in the sky – i.e. shortest days with lowest sun elevation and longest days with the sun's highest elevation. The optical efficiency is a function of the sun's elevation and azimuth. An example of the model is shown in Figure 6, where the pink circles represent the simulated points in time, and each 'horseshoe' of circles represents a full day.

All solar irradiation data used for modelling is from Meteonorm version 7.3 [25].

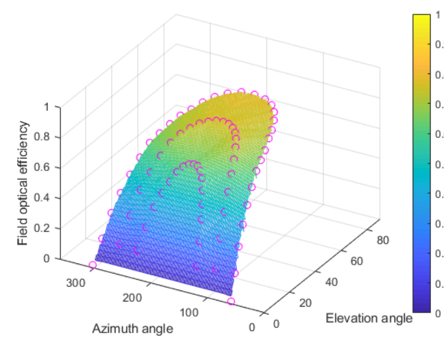

Figure 5: Efficiency map constructed by interpolating simulated days.

4.4 Energy model

The energy model is implemented as a pseudo steady-state model. The solar resource and optical efficiency is assumed steady with hourly resolution.

Once the optical model has generated the optical efficiency interpolation model, an annual simulation is completed to determine the energy available to the receiver for every hour in the year. The incident power on the receiver at time-step *i*, $\dot{Q}_{rec_i}$, is defined as follows:

$$\dot{Q}_{rec_i} = \eta_{opt_i} \dot{q}_{dni_i} A_{sf}, \quad (2)$$

where η_{opt_i} is the optical efficiency, $\dot{q}_{dni_i}$ is the DNI available for the specific time-step *i* (this is retrieved from a TMY weather file) and A_{sf} is the aperture area of the solar field, the reflector surface area. The receiver is modelled with the assumption that it is capable of heating the particles to 900 °C across its flux operating range as discussed in section 3.2.

The TES energy is modelled as an energy flow into and from storage, this follows the modelling approach used by Wagner [24] and Sioshansi and Denholm [26]. Equation 3 defines the energy available in storage at time-step i, E_{TES_i}:

$$E_{TES_i} = \eta_{rec_i} \cdot \dot{Q}_{rec_i} \cdot \Delta t + \eta_{TES} \cdot E_{TES_{i-1}} - \dot{x}_{i-1} \cdot \Delta t, \quad (3)$$

where $\dot{x}_{i-1}$ is the discharge from storage, Δt is the time-step for which all variables are assumed steady, η_{rec_i} is the thermal efficiency of the receiver and is a function of the incident solar flux as shown in Figure 2. η_{TES} is an efficiency parameter used to account for hourly heat losses from storage, this follows the modelling approach of Sioshansi and Denholm [26] and Lubkoll et al [8].

In order to ensure ore is always preheated, thermal energy is either provided from the TES or from electrical backup heaters. Equation 4 defines the source of thermal energy output for preheating at each time-step:

$$\dot{Q}_{out} = \dot{x}_i + \dot{Q}_{elec_i} \quad (4)$$

where $\dot{Q}_{elec_i}$ is the thermal output delivered from the back-up electrical heaters. The magnitude of TES discharge and/or electrical power for each time-step is determined by the dispatch optimization, which is discussed in section 5.

4.5 Economic model

After the optical and energy models have determined the thermal energy dispatch profile for a specific plant configuration an economic model is used to determine the combined solar-electric LCOH. LCOH is performance indicator analogous to levelized cost of electricity. The LCOH is the total life-cycle cost divided by the total life-cycle energy production – discounted to the present day. The LCOH parameter allows direct comparison of various technologies irrespective of scale, time period of investment or operating strategies [27].

From Short et al [27], with the assumption that the annual system output will remain steady over the lifetime of the plant, levelized cost of solar heat, $LCOH_s$, can be simplified to:

$$LCOH_s = \frac{\left(\frac{k_d(1+k_d)^n}{(1+k_d)^n - 1} + k_{ins}\right) \times CAPEX + O\&M}{Q_s}, \quad (5)$$

where k_d is the discount rate, n is the plant lifetime, k_{ins} is the insurance rate, CAPEX is the total capital expenditure, O&M is the operating and maintenance costs and $Q_s = \sum_{i=1}^{8760} \dot{x}_i$ is the sum of all annual solar energy output.

Table 3 provides the costs parameters for the solar system.

Table 3: Solar plant economic parameters.

CAPEX	Value
Heliostat[2]	112.5 $\$\cdot m^{-2}$
Receiver[1]	138 130 $\$\cdot m^{-2}$
Verticle particle transport[1]	140 892 \$ per tower
Horizontal particle transport	248 634 \$ per tower
Tower[1]	$8288+1.73\cdot h_{tower}^{2.75}$ \$ per tower
Thermal energy storage[1]	20 443 $\$\cdot MWh_{th}^{-1}$
Particle-to-air heat exchanger[1]	138 130 $\$\cdot MW_{th}^{-1}$
Indirect costs[1]	22 % of CAPEX
O&M[1]	3.9 % of CAPEX
Insurance rate[1]	1 % of CAPEX
Discount rate[2]	7 % of CAPEX

[1] from [6] in 2019 Dollars, [2] from [8].

The levelized cost of electrical heat, $LCOH_e$, is simplified to the cost of purchased electrical energy divided by the amount of energy bought. The reason for neglecting the cost of capital is that the 'fuel' cost is expected to greatly exceed the capital cost, as electric heaters are relatively inexpensive. The $LCOH_e$, is calculated as:

$$LCOH_e = \frac{\sum_{i=1}^{8760} \dot{Q}_e \cdot C_i}{Q_e}, \quad (6)$$

where $\dot{Q}_e$ is the required electrical energy at time-step i , C_i is the electrical tariff at time-step i and Q_e is the total annual electrical energy required.

The combined solar-electric LCOH, $LCOH_{comb}$, is the weighted average of $LCOH_e$ and $LCOH_s$ in terms of energy generation:

$$LCOH_{comb} = \frac{LCOH_e \cdot Q_e + LCOH_s \cdot Q_s}{Q_e + Q_s}. \quad (7)$$

5. DISPATCH OPTIMIZATION

The purpose of the dispatch optimization is to determine the dispatch of energy from TES for every time-step so as to minimize the cost of backup electrical heat. The benefit of TES is that it allows an increased solar capacity factor and also decouples the use of solar energy from the availability of the solar resource. This, coupled with the need to deliver steady thermal output, by means of back-up electrical heaters and a time-of-use electrical tariff creates the optimization problem.

Figure 7 shows the time-of-use electric tariff and the available solar energy from the receiver over the same time period. The tariff shown is the South African electrical utility, Eskom's, Megaflex tariff. This tariff is applicable to energy intensive industrial consumers. It can be seen that the solar resource availability does not coincide with peak electrical price periods. The goal of the dispatch optimization is to use the TES to shift the use of lower cost solar energy to coincide with periods when the tariff is highest. So as to ensure that when electrical backup heat is required, it is used only when the tariff is lowest.

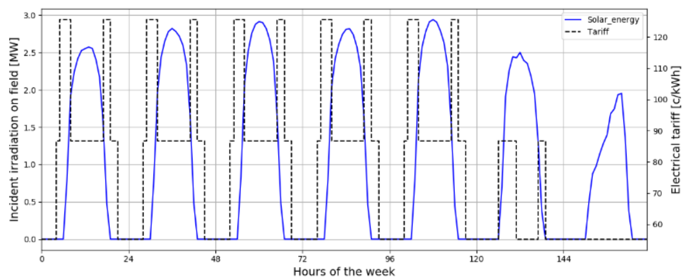

Figure 6: Time-of-use tariff and available solar resource over a week.

5.1 Optimization problem formulation

The objective of the optimization problem is to minimize the cost of electrical backup heat for the entire year:

$$\min\left\{\sum_{i=1}^{8760}\left[\dot{Q}_{out}-\dot{x}_i\right]\times C_i+\rho\sum_{i=1}^{8759}\left[\dot{x}_i-\dot{x}_{i+1}\right]^2\right\}, \qquad (8)$$

where $\dot{Q}_{out}$ is the constant thermal demand for preheater, $\dot{x}_i$ is the discharge from storage and is also the design variable, C_i is the electrical tariff and ρ is a penalty parameter.

The terms in the first bracket, the difference between the required heat and the solar-derived heat discharged from storage, represent the electrical heat required at time step *i*. This is Equation 4 re-arranged. The second term is a penalty function that is added to produce a smoother dispatch profile. Without the penalty the dispatch profile can fluctuate over periods of constant electrical tariff for certain initial guesses. This was deemed unrealistic as this equates to rapidly cycling the backup electrical heaters on and off. The penalty function is the cumulative sum of successive gradients of the dispatch profile. The greater the rate of change of the gradient, the worse the effect of the penalty on the objective function value, thereby favoring a smoother profile.

The objective function is subject to two constraints that enforce the system's energy balance:

$$E_{TES_i}-\dot{x}_i\cdot\Delta t\ \geq 0 \qquad (9)$$

$$\dot{Q}_{out}-\dot{x}_i\ \geq 0 \qquad (10)$$

Equation 9 ensures the maximum discharge does not exceed the energy content in storage. Equation 10 ensures the maximum discharge does not exceed the energy required by the preheater.

In this optimization problem C_i and $\dot{Q}_{out}$ are known inputs, $\dot{x}_i$ has some initial guess which is then updated iteratively the optimizer and E_{TES_i} is calculated from the energy balance of equation 3. All variables for the optimization problem are shown on the plant schematic in Figure 3.

5.2 Optimization solvers

Various open source and commercial solvers are tested on the problem. The open sources solvers are from the Python scientific computing library Scipy[28] and the commercial solvers are from Vanderplaats Research and Development's DOT software[29].

Due to the curse of dimensionality (a full year with hourly resolution has 8760 design variables) the optimizers could not effectively solve the dispatch profile for a full year. The various optimizers are therefore tested on a smaller 3000 design variable (ie 3000 hours or 125 days of dispatch optimization) problem. This provides an indication of which solvers are well suited to this specific problem and its solution space.

Table 4 presents the results of the various optimizers on the 3000 design variable problem. The result of the optimization is compared to an heuristic operating strategy used by Lubkoll et al [8] and Hockaday et al [30] to provide an indication of the improvements achieved. The heuristics strategy outputs to the process when sufficient energy is available from the receiver and/or TES, together or separately, to meet the full process demand. Then electrical heat is filled in where needed to meet the constant preheating thermal load.

From Table 4 it can be seen the SLP and SLSQP solvers performed comparably, and substantially better than the other solvers in terms of achieved objective function value. It is noted that all the commercial solvers successfully converged whereas the open source solvers terminated at the maximum allowed iterations. The commercial solvers proved more robust in terms of infeasible starting positions. For these reasons the SLP solver was selected for future work.

Table 4: Single time-horizon optimization of a 3000 hour / design variable problem.

Solver	Source	Execution time	Normalized object function value[1]	Relative difference[2]
MMFD	DOT	1620 s	1.095	+9.5 %
SLP	DOT	16324 s	0.840	-15.9 %
SQP	DOT	677 s	1.293	+29.3 %
Trust-constr	Scipy	37111 s	1.699	+69 %
SLSQP	Scipy	7756 s	0.836	-16.4 %
Heuristic	[8]	-	1	-

[1] normalized by heuristic strategy's value, 2 relative difference to the heuristic objective function value.

5.3 Rolling time-horizon optimization

As none of the solvers could complete the full scale optimization problem a different approach is required. A rolling time-horizon approach is implemented to overcome the dimensionality issue. This approach optimizes the full 365 day problem, one day at a time, and then combines the results into an annual dispatch profile. However this would produce a poor dispatch profile if single days are optimized without knowledge of future trends in available resource and electric tariff. Therefore one day is optimized with a time-horizon longer than 24 hours, but only the first 24 hours is kept towards the final dispatch profile. This way the optimizer can hold back low cost energy in TES to meet future demand during high electric tariff periods. This approach was implemented by Sioshansi and Denholm [31] and by Wagner [24].

Figure 7 shows the solar resource profile, TES amount and TES discharge profile for a single optimized day, with no future knowledge of solar resource or tariff. At the end of the 24 hours the TES is depleted, as using all available solar resource minimizes the cost of electrical heat over this period. The consequence of this is that expensive electrical heat will be required to meet the early morning demand for the next day – see the time-of-use profile in Figure 7.

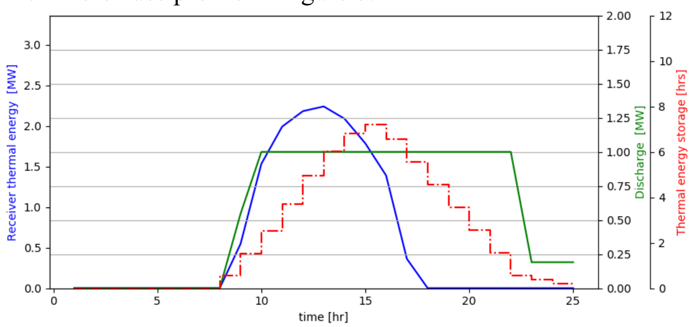

Figure 7: Single day optimization with a 24 hour time-horizon.

Figure 8 shows the same information but for a 72 hour time-horizon. It can now be seen that the TES is not depleted at the end of the first 24 hours. Some solar energy is held back overnight (see hours 25 - 30), while the electrical tariff is low, to meet the demand the next morning when the electrical tariff is high. Thereby minimizing the cost of backup electrical heat. In other words, the solar heat is used when it is the most valuable – replacing high cost electrical energy. Not shown in these figures is that to meet the constant heat demand the difference between the TES discharge and the required constant preheater demand will be supplied by electrical heat.

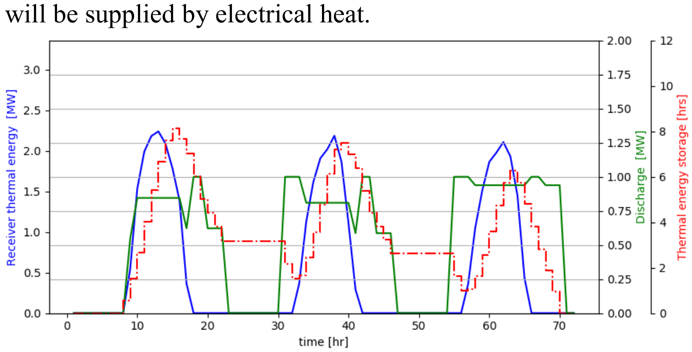

Figure 8: Single day optimization with a 72 hour time-horizon.

Figure 7 and 8 depict the importance of optimizing each day with a longer time-horizon. From Figure 8, only the first 24 hours would be saved and go toward the final dispatch profile. The dispatch optimization algorithm would then step forward one day and optimize again with the extended time-horizon. The amount of energy available in storage after the 24th hour is carried over from one day to the next, as the algorithm steps forward in time. This ensures a continuous dispatch profile is constructed from discrete optimization steps. This process is completed for all 365 days.

In order to determine a suitable time-horizon length a parametric study is completed. The entire year is optimized by means of the rolling time-horizon approach, with each iteration using a different time-horizon length. The results of this study are shown in Figure 9. Convergence is reached with a time-horizon of 80 hours.

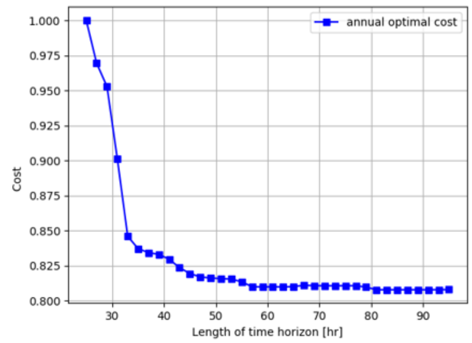

Figure 9: Parametric study to determine suitable time-horizon length.

5.4 Results of rolling time-horizon

Implementation of the rolling time-horizon approach results in the capability to optimize the dispatch profile for the entire year. Additionally the execution time is dramatically decreased as the solution space for the many smaller optimization problems are simpler to solve. The same 3000 design variable problem, from Table 4, is solved using the rolling time-horizon approach for comparison. These results are shown in Table 5.

Table 5: Rolling time-horizon optimization of a 3000 hour / design variable problem.

Parameter	Value
Solver	SLP
Time-horizon	80 hours
Execution time	48.2 s
Normalized objective value	0.856
Relative Execution time difference*	-99.7 %
Relative objective function difference*	+1.9 %

*Relative difference to SLP results from table 4

An example of an optimized TES dispatch profile for a modelled CST plant is shown in Figure 10. The dispatch profile is shown in green and the electrical tariff in black. This is for hours 4000 to 4200 of the year. It can be seen that the TES dispatch coincides with peak tariff periods, within the constraints of the available resource. During periods of low tariff prices the required

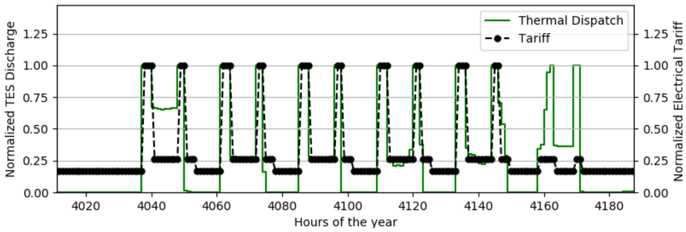

Figure 10: Example of an optimized TES dispatch profile.

6. CASE STUDY

This section describes a scenario for a future smelter development in a region that would benefit from CST preheating of Manganese ore. The case study provides the necessary details from which a CST plant can be sized and modelled using the methodology previously discussed.

The case study is for a 30 MW_e furnace operating at 40 t/hr and where the ore is preheated to 600 °C. Modelling for the PREMA project by Hockaday et al [30] has determined this would require a 13.6 MW_{th} preheater unit.

The location for the envisaged smelter is near Hotazel, Northern Cape, South Africa. This is where the Kalahari Manganese Field is found, which contains 99 % of South Africa's Manganese reserves. This equates to 80 % of the global land based Manganese reserves [9]. Figure 11 shows a DNI map of South Africa, the smelter is envisaged to be located at the indicated yellow star, in a region of very high annual DNI. Currently no smelter is located in this region as seen in Figure 12. Rail infrastructure exists to the Manganese export terminals at Saldanha Bay and Port Elizabeth as seen in Figure 13. Furthermore these lines are currently being upgrading [32]. South Africa exports the majority of its Manganese as ore, before any beneficiation process making the investment in more smelters an attractive proposition. The combination of solar resource, existing transport infrastructure and the location of the Manganese ore makes an attractive location for a CST preheated Manganese smelter.

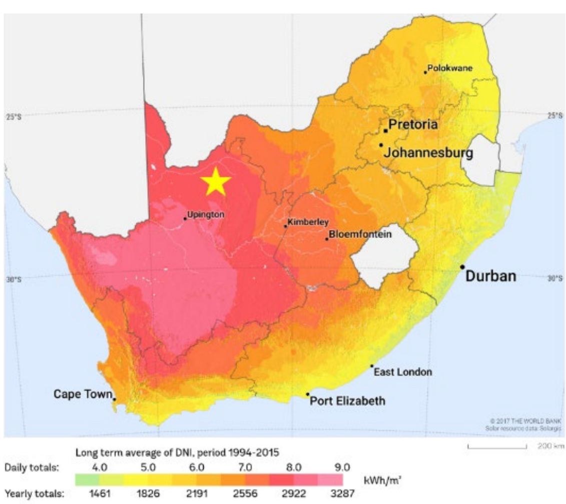

Figure 11: Direct Normal Irradiance map of South Africa [21].

Figure 12: Location of Manganese smelters in South Africa [9].

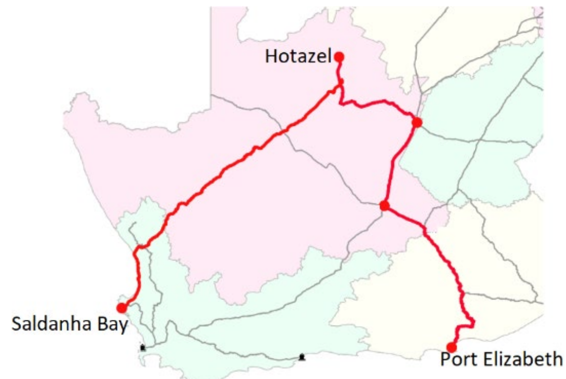

Figure 13: South Africa rail infrastructure [33].

7. RESULTS

The CST plant is sized to deliver the lowest $LCOH_{comb}$ for one tower with 2.5 MW_{th} a CentRec® receiver. As this is insufficient to meet the full preheater thermal demand multiple tower and solar fields will be required. This follows the approach of Amsbeck et al [6] for thermal requirements greater than the rated load of the commercial CentRec® receiver.

The lowest $LCOH_{comb}$ is determined through a parametric study. The amount of TES and the solar multiple are varied and the resulting $LCOH_{comb}$ is determined for each plant configuration. The parametric study results can be seen in Figure 14. The lowest cost system consists of a solar multiple of 3 with 14 hours of TES.

The final single tower system consists of a solar multiple of 2.94 with a corresponding output to process of 0.85 MW_{th}. This selection is made so an integer number of towers satisfy the 13.6 MW_{th} preheater thermal demand. A total of 16 towers will be required, for a total land use of 57 008 m^2. A single CST tower plant delivers 5375 MWh_{th} per year, this corresponds to a solar share of 72 % of the total required energy for the preheater. The rest being supplied by the electrical heaters.

$LCOH_{e,total}$ represents the scenario where the preheater thermal demand is met by only electrical heat. This can be seen as equivalent to no preheating occurring and the furnace itself delivering this energy. The economic benefit of the CST-electric hybrid preheating is compared to no preheating by comparing $LCOH_{comb}$ and $LCOH_{e,total}$. The combined solar-electric systems delivers heat with a 100 % capacity factor for 35.80 % lower cost per unit heat, compared to full electric heating.

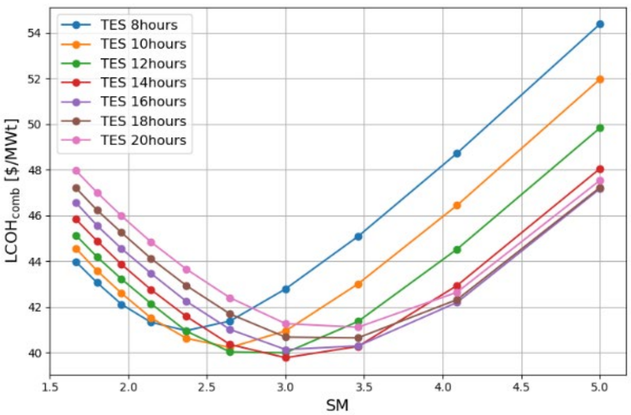

Figure 14: TES and SM parametric study.

The environmental benefit for preheating Manganese ore to 600 °C by means of a CST plant is a 7 % reduction in CO2 production for the smelting process compared to no preheating, as determined by the furnace process modelling of Hockaday et al [30]. Further benefit can be gained from the reduction in electricity required by the smelting process if the electricity is fossil fuel derived.

The results of the case study are summarized in Table 6.

Table 6: Case study results.

	Parameter	Value
Furnace	Furnace rating	30 MW_e
	Preheater rating	13.6 MW_{th}
	Ore preheated temperature	600 °C
Site data	Latitude	-27.24 S
	Longitude	22.902 E
	Annual DNI	2796 $kWh \cdot m^{-2}$
Single tower CST plant	$A_{sf,single}$	3563 m^2
	$\eta_{opt,a}$	65 %
	TES	14 hours
	SM	2.94
	$\dot{Q}_{proces}$	0.85 MW_{th}
	$Q_{s,a}$	5375 MWh_{th}
Total solar plant	Towers	16
	$A_{sf,total}$	57 008 m^2
Economics	$LCOH_s$	38.90 $\$ \cdot MWh_t^{-1}$
	$LCOH_e$	42.13 $\$ \cdot MWh_t^{-1}$
	$LCOH_{comb}$	39.80 $\$ \cdot MWh_t^{-1}$
	$LOCH_{e,total}$ [1]	62.00 $\$ \cdot MWh_t^{-1}$
	Savings [2]	35.88 %

[1] calculated using equation 2 for all required energy delivered by electrical power.
[2] relative difference between $LOCH_{e,total}$ and $LCOH_{comb}$

8. CONCLUSION

This paper described the development of an optical, energy and economic model for a hybrid CST-electric plant used for providing thermal heat to preheat Manganese ore before smelting. To constantly deliver preheated ore the plant relies on backup-electric heaters. The work occurs in a locations where the electrical market follows a time-of-use tariff. The cost of electrical heat was then minimized by optimizing the time at which the TES discharged. This is achieved by using lower cost solar derived heat when the electrical tariff is high.

This model was used to investigate the economic benefit of incorporating CST technologies in the energy intensive Manganese smelting industry.

A case study for a Manganese smelter, preferentially situated in the high DNI region of the Northern Cape, South Africa with an accompanying CST plant was developed. The purpose of the case study was to determine the economic benefit of the CST-electric plant delivering thermal energy for preheating. The results proved the effectiveness of CST technologies for delivering high temperature process heat at lower cost than alternate fuel sources. This is due to the good solar resource of the selected region, and increased competiveness of the technology when thermal energy is required rather electricity. When CST technologies are used to generate electricity the thermal to electrical conversion is limited by the Carnot efficiency, and the associated energy loss is significant. Without this thermal to electric loss CST technologies can improve their competitiveness as a larger percentage of the intercepted solar energy can be utilized for the end product. The economics improve as the capital cost of the technology is distributed over more energy for the same sized CST plant.

ACKNOWLEDGEMENTS

The PReMA project has received funding from the European Union's Horizon 2020Research and Innovation Programme under Grant Agreement No 820561.

REFERENCES

[1] Murdock, H. E. *et al.*, "Renewables 2019 Global Status Report," 2019.

[2] Lovegrove, K. and Stein, W., *Concentrating solar power technology : principles, developments and applications*. Cambridge, UK : Woodhead, 2012.

[3] Tangstad, M., Ichihara, K. and Ringdalen, E., "Pretreatment unit in ferromanganese production," *INFACON XIV*, pp. 99–106, 2015.

[4] A.SPIRE, "Energy efficient, primary production of manganese ferroalloys through the application of novel energy systems in the drying and pre-heating of furnace feed materials.," 2015. [Online]. Available: www.spire2030.eu/prema. [Accessed: 11-Dec-2019].

[5] Ho, C., "A review of high-temperature particle receivers for concentrating solar power," *Appl. Therm. Eng.*, vol. 109, pp. 958–969, 2016.

[6] Amsbeck, L., Behrendt, B., Prosin, T. and Buck, R., “Particle tower system with direct absorption centrifugal receiver for high temperature process heat,” in *SolarPACES conference*, 2014.

[7] Amsbeck, L., Buck, R. and Prosin, T., “Particle tower technology applied to metallurgic plant and peak-time boosting of steam power plants.,” in *SolarPaces*, 2015.

[8] Lubkoll, M., Hockaday, S. A. C., Harms, T. M. and von Backstrom, T. W., “Integrating solar process heat into manganese ore pre-heating,” in *Conference Proceedings: 5th Southern African Solar Energy Conference*, 2018.

[9] Steenkamp, J. D. and Basson, J., “The manganese ferroalloys industry in southern Africa,” *J. South. African Inst. Min. Metall.*, vol. 113, no. 8, pp. 667–676, 2013.

[10] “Helio100,” 2018. [Online]. Available: www.helio100.sun.ac.za. [Accessed: 11-Dec-2019].

[11] Wu, W., Trebing, D., Amsbeck, L., Buck, R. and Pitz-Paal, R., “Prototype testing of a centrifugal particle receiver for high-temperature concentrating solar applications,” *J. Sol. Energy Eng. Trans. ASME*, vol. 137, no. 4, 2015, doi: 10.1115/1.4030657.

[12] Wu, W., Uhlig, R. and Pitz-Paal, R., “Numerical simulation of a centrifugal particle receiver for high-temperature concentrating solar applications,” *Numer. Heat Transf.*, vol. 68, pp. 133–149, 2015.

[13] Wu, W., Amsbeck, L., Buck, R., Uhlig, R. and Ritz-Paal, R., “Proof of concept test of a cetrifugal particle receiver,” in *SolarPACES*, 2013.

[14] Ebert, M. *et al.*, “Operational experience of a centrifugal particle receiver prototype.,” in *SolarPACES*, 2018.

[15] Ho, C. K. *et al.*, “Highlights of the high-temperature falling particle receiver project: 2012-2016,” in *AIP Conference Proceedings*, 2017, vol. 1850, no. 1, p. 30027.

[16] Erbert, M. *et al.*, “Operational experience of a centrifugal particle receiver prototype,” in *SolarPACES*, 2018.

[17] Palacios, A., Barreneche, C., Navarro, M. E. and Ding, Y., “Thermal energy storage technologies for concentrated solar power A review from a materials perspective,” *Renew. Energy*, 2019, doi: 10.1016/j.renene.2019.10.127.

[18] El-Leathy, A. *et al.*, “Experimental study of heat loss from a thermal energy storage system for use with a high-temperature falling particle receiver system,” in *SolarPaces*, 2013.

[19] Al-Ansary, H., Djajadiwinata, E., El-Leathy, A., Danish, S. and Al-Suhaibani, Z., “Modelling of transient cyclic behavior of a solid particle thermal energy storage bin for central receiver applications.,” in *SolarPaces*, 2014.

[20] Hertel, J. *et al.*, “Development and Test of a Direct Contact Heat Exchanger (Particle-Air) for Industrial Process Heat Applications,” in *ASME 2019 13th International Conference on Energy Sustainability collocated with the ASME 2019 Heat Transfer Summer Conference*, 2019.

[21] Amsbeck, L., Buck, R., Rehbock, T., Prosin, T. and Schwarzbözl, P., “Solar sludge drying demonstration plant,” in *4 th International Symposium on Innovation and Technology in the Phosphate Industry*, 2015.

[22] Blanco, M., Mutuberria, A. and Martinez, D., “Experimental validation of Tonatiuh using the Plataforma Solar de Almería secondary concentrator test campaign data,” *Proc. SolarPACES*, 2010.

[23] Stine, W. B. and Geyer, M., “Power from the sun.,” 2001. [Online]. Available: http://www.powerfromthesun.net/book.html. [Accessed: 10-Apr-2018].

[24] Wagner, M. J., “Optimization of stored energy dispatch for concentrating solar power systems,” Colorado School of Mines. Arthur Lakes Library.

[25] Meteotest-AG, “Meteonorm.” [Online]. Available: www.meteonorm.com.

[26] Sioshansi, R. and Denholm, P., “The value of concentrating solar power and thermal energy storage,” *IEEE Trans. Sustain. Energy*, vol. 1, no. 3, pp. 173–183, 2010, doi: 10.1109/TSTE.2010.2052078.

[27] Short, W., Packey, D. J. and Holt, T., “A manual for the economic evaluation of energy efficiency and renewable energy technologies,” National Renewable Energy Lab., Golden, CO (United States), 1995.

[28] Oliphant, T. E., “Python for Scientific Computing,” *Comput. Sci. Eng.*, vol. 9, no. 3, pp. 10–20, 2007, doi: 10.1109/MCSE.2007.58.

[29] Development, V. R. and, “DOT optimization.” [Online]. Available: http://www.vrand.com/products/dot-optimization/.

[30] Hockaday, L., Mckechnie, T., von Puttkamer, M. N. and Lubkoll, M., “The impact of solar thermal resource characteristics on solar thermal preheating of manganese ores,” in *The Minerals, Metals and Materials Society 149th Annual Meeting and Exhibition*, 2020.

[31] Madaeni, S. H., Sioshansi, R. and Denholm, P., “How Thermal Energy Storage Enhances the Economic Viability of Concentrating Solar Power,” *Proc. IEEE*, vol. 100, no. 2, pp. 335–347, 2012, doi: 10.1109/JPROC.2011.2144950.

[32] Transnet, “Freight Rail 2018,” 2018. [Online]. Available: https://www.transnet.net/InvestorRelations/AR2018/TFR.pdf.

[33] Transnet, “Transet long term planning framework,” 2017. [Online]. Available: www.transnet.net/BusinessWithUs/Pages/LTPF.aspx.

